



Structure and photoluminescence characteristics of mixed nickel–chromium oxides nanostructures

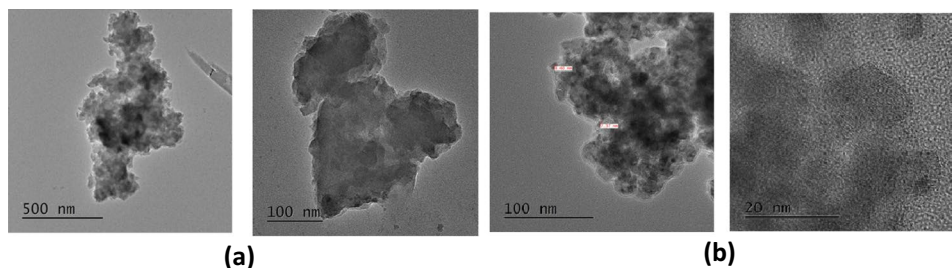
M. Sh. Zoromba^{1,2} · M. Bassyouni^{1,3} · M. H. Abdel-Aziz^{1,4} · Ahmed F. Al-Hossainy^{5,6} · Numan Salah⁶ · A. A. Al-Ghamdi⁷ · Mohamed R. Eid^{8,9}

Received: 18 February 2019 / Accepted: 13 August 2019 / Published online: 22 August 2019
© Springer-Verlag GmbH Germany, part of Springer Nature 2019

Abstract

In this work, nickel–chromium-layered double hydroxide (Ni(II)–Cr(III)LDH) is prepared via co-precipitation method at room temperature with 1:2:3 molar ratio of $\text{CrCl}_3 \cdot 6\text{H}_2\text{O}$: $\text{NiCl}_2 \cdot 6\text{H}_2\text{O}$: NaCl using sodium hydroxide as a precipitating agent. Ni(II)–Cr(III) LDH is synthesized in the absence and in the presence of functionalized amino-organic compounds such as acetamide, glycine, and urea. The ratio between $\text{CrCl}_3 \cdot 6\text{H}_2\text{O}$: $\text{NiCl}_2 \cdot 6\text{H}_2\text{O}$: NaCl : acetamide, glycine or urea was 1:2:3:6. The mixed nickel–chromium oxide nanoparticles are prepared by the calcination of Ni(II)–Cr(III) LDHs at 600 °C for 2.5 h. Ni(II)–Cr(III) LDHs and mixed Ni(II)–Cr(III) oxides nanoparticles are characterized by several techniques including FTIR, TGA, XRD, FESEM, HRTEM, and PL. Functionalized amino-organic compounds improve the thermal stability in the order of glycine > urea > acetamide. Also, it affects photoluminescence PL intensity which indicates a marked reduction in electron–hole recombination with the highest photocatalytic activity compared to visible light-driven H_2 and O_2 evolution. The resulting mixed Ni(II)–Cr(III) oxides particles have an amorphous structure and a relatively uniform size of below 10 nm.

Graphic abstract



HRTEM images of Ni(II)–Cr(III)/g LDH at two different magnifications: a) before and b) after calcination

1 Introduction

The layered crystalline configuration of layered double hydroxides (LDHs) contains various intercalating anionic units with the ability to exchange these interlayer anions with relatively larger anionic organic residues. The main

character of these mixed metal oxides is considered more complete for the MgAl-CO_3^{2-} structure. LDHs have three unequal types of base locations, namely; strong basic O_2 sites present on the surface of the material, medium basic O sites, and the hydroxyl groups that give rise to locations with weak basicity. The variability in chemical structure and physico-chemical characteristics of synthesized LDHs compromises excessive diversity in applications of these materials. The creation of active base sites leads to the remarkable increase in catalytic reactivity after application of the calcination process. This intercalation makes LDHs

✉ M. Sh. Zoromba
mzoromba@kau.edu.sa

✉ Ahmed F. Al-Hossainy
ahmed73chem@scinv.au.edu.eg

Extended author information available on the last page of the article

very beneficial in various uses such as nanofillers for the production of polymer nanocomposites, and in nanotechnology, to develop the flame retardancy of polymer nanocomposites [1]. The unique properties of these materials open up the field in many applications such as the use of adsorption of harmful ions in the environment, which accompany dilute water residues [2]. It can also be used in disposing of nuclear waste by adsorption such as anionic radionuclides. In addition, it can be used for storage purposes by converting it into insoluble materials such as ceramics [3]. Calcination of synthetic LDHs produces mixed metal oxides (MMOs) with strong basic properties and large surface areas compared to the original LDH precursor. The synthesis of many organic entities is possible by controlled calcination of LDHs, such as methane or hydrocarbon steam reforming, aldol, condensation methanation, epoxidation [1–4], and nitrous oxide (N_2O) decomposition [5, 6]. In general, LDHs are weak, solid bases, and achieve improved basic properties when stimulated primarily by thermal calcination [7, 8]. Both LDHs and calcined LDHs have different applications in many fields, including catalysis [9], pharmaceutical products [10], polymer additives [11], environmental cleaning by ion exchange or adsorption processes [12, 13], selective chemical, non-reactors [14], in separation and membrane technology [15], and as photoactive materials [16]. LDHs have low costs, making their use and MMOs as solid catalysts a promising alternative for the refinement of soil, groundwater, and waste water [17, 18]. On the other hand, there is a variety of morphologies of LDHs, it has different forms such as powders [19, 20], and spheres [21, 22], LDH belt with nanoparticles [23] and fibrous structure [24]. Progress in the production of LDH structural ingredients with dissimilar morphologies of powder/sphere, mono/mono (1-D) belt/fiber; to two-dimensional films was reported by Ye Kuang et al. [25]. On the other hand, synthesis of various oxides, nanoparticles, including iron, nickel, cobalt, copper, and chromium was reported by thermal decomposition [23, 26–30].

This study aims to investigate the thermal stability, morphology, and crystallinity of such prepared Ni(II)–Cr(III) LDH in the absence and in the presence of functionalized amino-organic compounds (acetamide, glycine, and urea). The aim of the study is also to prepare mixed nickel–chromium oxides nanostructures via easy thermal decomposition of LDHs.

2 Experimental

2.1 Raw materials

All chemicals, glycine (Aldrich), acetamide (Aldrich), urea (Aldrich), sodium chloride (Merck), sodium hydroxide

(Merck), nickel chloride hexahydrate (Sigma), chromium chloride hexahydrate (Sigma) were employed as received without further refinement.

2.2 Synthesis of LDHs

The synthesis process of LDH was done at room temperature by means of the method of co-precipitation using a molar ratio of $CrCl_3 \cdot 6H_2O:NiCl_2 \cdot 6H_2O:NaCl = 1:2:3$. Typically, 5.32 g of $CrCl_3 \cdot 6H_2O$ was dissolved in a reasonable volume of distilled water. 9.5 g of $NiCl_2 \cdot 6H_2O$ was supplied to the chromium solution under magnetic stirring at 850 rpm. 3.5 g NaCl as a host material was added to the mixture. The Ni(II)–Cr(III) mixture volume reaches 200 ml by adding distilled water. Sodium hydroxide (25% wt./wt.) was added dropwise until the pH reached 10.5. Gradually Ni(II)–Cr(III) LDH was precipitated by the addition of sodium hydroxide solution. The resulting slurry of Ni(II)–Cr(III) LDH was left in a water bath for 24 h at 75 °C. The filtration process was applied for the Ni(II)–Cr(III) LDH followed by washing several times by means of distilled water to eliminate extra solvable ions, until pH of filtrate reached 7. The drying is achieved in an oven at 80 °C. The resulting sample was labeled with Ni(II)–Cr(III) LDH. The same procedure was repeated in the presence of acetamide, glycine, and urea. The ratio between $CrCl_3 \cdot 6H_2O: NiCl_2 \cdot 6H_2O: NaCl: acetamide, glycine$ or urea was 1:2:3:6. The resulting Ni(II)–Cr(III) LDHs that were prepared in absence and in the presence of acetamide, glycine, and urea were labeled by Ni(II)–Cr(III) LDH, Ni(II)–Cr(III)/a LDH, Ni(II)–Cr(III)/g LDH, and Ni(II)–Cr(III)/u LDH, respectively.

2.3 Synthesis of mixed Ni(II)–Cr(III) oxides nanoparticles

The mixed metal oxide nanoparticles of chromium and nickel were prepared from Ni(II)–Cr(III) LDHs by calcination at 600 °C for 2.5 h.

2.4 Characterization

Characterization methods and typical conditions are recorded in Table 1.

3 Results and discussion

3.1 FTIR analysis of Ni(II)–Cr(III) LDHs

The FT-IR analysis was used to demonstrate that the organic molecules acetamide, glycine, and urea molecules were successfully introduced into the LDHs and that FT-IR analysis can ensure the existence of interlayer

Table 1 List of characterization methods

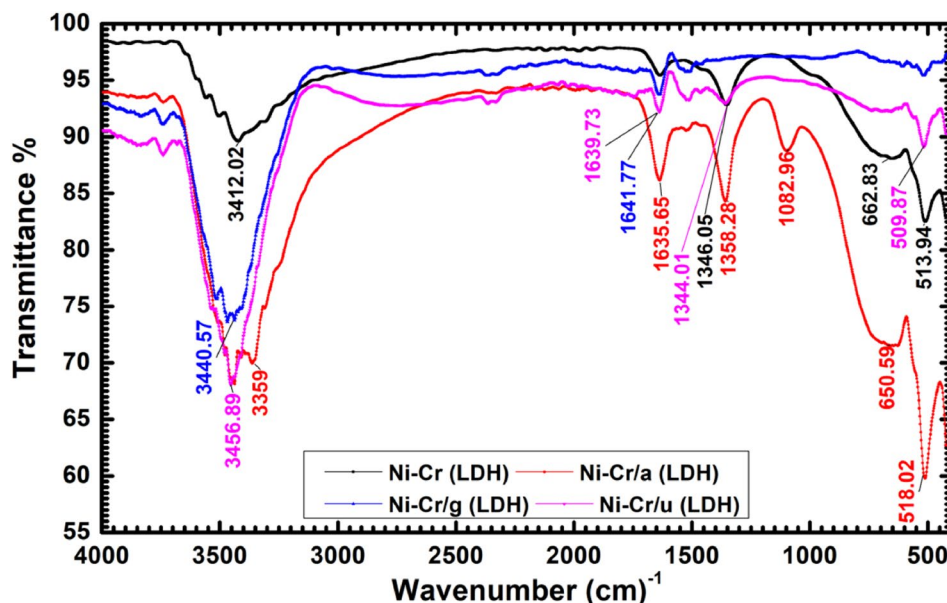
Characterization method	Model used and conditions
XRD	Philips X'Pert, CuK α , 40 kV, 30 mA and $k = 1.54056 \text{ \AA}$
HRTEM	TEM, JEOL ARM-200F, JEOL, Japan
Photoluminescence (PL)	RF-5301 PC, Shimadzu. The excitation wavelength was 325 nm. The excitation and emission slits width was fixed at 10 nm
FTIR	PerkinElmer FT-IR type 1650 spectrophotometer (wavelength range 4000–200 cm^{-1})
TGA	PerkinElmer Thermogravimetric Analyzer TGA 4000 was employed Temperature range is 50–995 $^{\circ}\text{C}$ and heating rate is 10 $^{\circ}\text{C}/\text{min}$ in nitrogen atmosphere
FESEM	FESEM, JSM-7500F, JEOL, Japan

anions, crystalline water, and lattice O_2 vibrations in LDHs. Figure 1 shows the FT-IR spectra of the samples prepared in this study. Figure 1a shows a broad band at 3412 cm^{-1} which can be attributed to stretching vibrations of OH ions or physically adsorbed water and also due to moisture absorption [31]. The weak band at 1639.73 cm^{-1} as shown in Fig. 1b can be ascribed to the bending mode of water molecules. In Fig. 1c, the weak band at 2450 cm^{-1} represents an extended vibration of NH bonds. Extended N–H vibrations in the absorption range at 518 cm^{-1} are associated with the stretching and bending patterns in the metal–oxygen bonds [32]. The absorption range at 1635 cm^{-1} , 1641 cm^{-1} , 1639 cm^{-1} for Ni(II)–Cr(III)/a, Ni(II)–Cr(III)/g, and Ni(II)–Cr(III)/u LDH accordingly belongs to the asymmetric expansion of the carbonyl group in acetamide, glycine, and urea as shown in Fig. 1d.

3.2 TGA of Ni(II)–Cr(III) LDHs

For assessment of the thermal stability of the LDHs, the temperature was fixed at 100 and 200 $^{\circ}\text{C}$ for 10 min during the thermal degradation process. This leads to two clear plateaus during the test as the weight decreases at constant temperature. Figure 2 shows that the thermal stability of LDHs is influenced by the presence of organic molecules and the effect varies in the order of glycine > urea > acetamide. The data in Fig. 2 show that the thermal strength of the LDHs structure reaches temperatures of about 200 $^{\circ}\text{C}$. Calcination above 200 $^{\circ}\text{C}$ decomposes LDHs into unstructured mixed metal oxides. The oxides obtained in this way are uniformly distributed (“solid solution”) for non-similar cations within the mixed oxide structure, which is a major motivation for the use of LDHs in catalysis applications, for example, as a catalyst support or catalyst precursor. The Ni(II)–Cr(III)/g LDH, Ni(II)–Cr(III)/u LDH, Ni(II)–Cr(III)/a LDH, and Ni(II)–Cr(III) LDH keep the same behavior at temperatures of 100 and 200 $^{\circ}\text{C}$ with the same above order. The loss of

Fig. 1 FTIR of a Ni(II)–Cr(III) LDH; b Ni(II)–Cr(III)/u LDH; c Ni(II)–Cr(III)/g LDH; and d Ni(II)–Cr(III)/a LDH



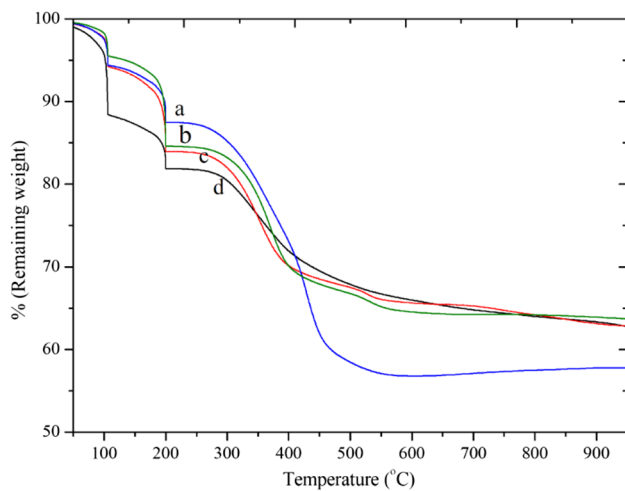


Fig. 2 TGA of a Ni(II)–Cr(III)/g LDH; b Ni(II)–Cr(III)/u LDH; c Ni(II)–Cr(III)/a LDH; and d Ni(II)–Cr(III) LDH

mass up to 200 °C is due to the elimination of interlayer and adsorbed water [33]. In the range of 250–500 °C, the breakdown of interlayer hydroxyl and chloride anions takes place. The existence of the transition metals in the LDHs samples presented negligible influence on the thermal strength. From Fig. 2, a temperature of 600 °C was selected for calcination of LDHs. The calcination temperature is crucial for effective reconstruction of the layered structure. The temperature

throughout the calcination of LDHs should be greater than the temperature of the layer breakdown and below than that of formation of spinel phase (this solid phase is stable and cannot be transformed to LDH in water). Consequently, the calcination temperature for LDHs is typically located between 400 and 700 °C [34].

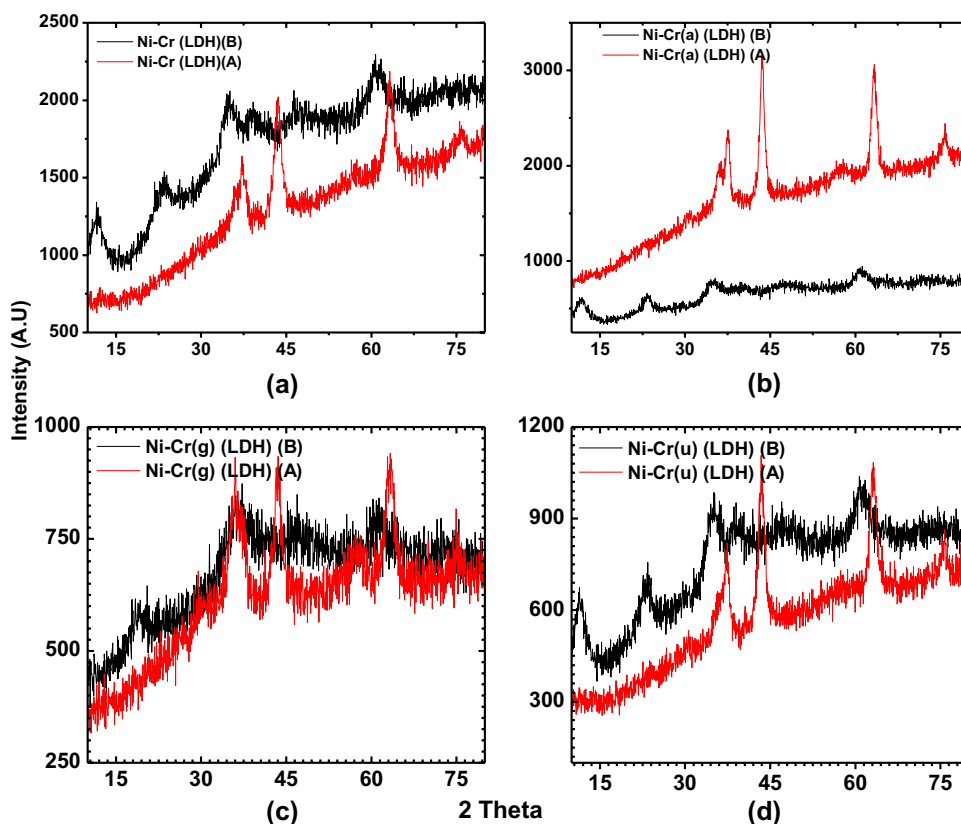
3.3 XRD diffraction of Ni(II)–Cr(III) LDH

The structural properties of the original Ni(II)–Cr(III) LDH before and after calcination with acetamide, glycine, and urea were inspected by X-ray diffraction technique. The XRD patterns for the Ni(II)–Cr(III) LDHs are shown in Fig. 3a–d. A glance at the XRD data listed in Table 2 indicated that six of titled compound afforded a Monoclinic 2 crystalline phase, space group $P2_1/m$, one a Tetragonal (Ni(II)–Cr(III) (LDH)B), space group $P4/m$, and Hexagonal (Ni(II)–Cr(III) (g) (LDH)A), space group $P6/m$ for the last compound. It demonstrates well-defined basic peaks having orientations in the (031) (103) (300) (140) (200) (222) (002), and (222) planes for investigated Ni(II)–Cr(III) LDH, Ni(II)–Cr(III)/a LDH, Ni(II)–Cr(III)/g LDH, and Ni(II)–Cr(III)/u LDH (before and after calcination), respectively. Among these planes in Ni(II)–Cr(III) LDHs before calcination, the (015) (628) (054) (034) surface at d -spacing, equal to 1.52 Å, with the maximum intensity, presents the smallest surface energy and is thermodynamically and

Table 2 XRD data of original Ni(II)–Cr(III) LDH before and after calcination with acetamide, glycine, and urea; symmetry (hkl) plans and their corresponding 2θ position and, d -spacing

Symmetry (before calcination)	2θ	(hkl)	d (Å)	Symmetry (after calcination)	2θ	(hkl)	d (Å)
Ni(II)–Cr(III) (LDH) [40] Monoclinic 2 (a : 8.43, b :70.9, c : 7.91 Å), $\gamma=90$, $\beta=90.25$, $\alpha=90^\circ$	11.86	031	7.46	Ni(II)–Cr(III) (LDH) [44] Tetragonal (a : 4.15, b : 4.15, c : 17.27 Å), $\gamma=90$, $\beta=90$, $\alpha=90^\circ$	37.01	114	2.43
	22.99	0161	3.86		43.54	200	2.08
	34.99	–371	2.56		63.26	101	1.47
	46.34	054	1.95		75.62	314	1.26
	60.96	015	1.52				
Ni(II)–Cr(III) (a) (LDH) [41] Monoclinic 2 (a : 23.69, b :3.98, c : 4.47 Å), $\gamma=90$, $\beta=93.90$, $\alpha=90^\circ$	11.76	103	7.52	Ni(II)–Cr(III) (a) (LDH) [45] Monoclinic 2 (a : 15.82, b :7.69, c : 7.44 Å), $\gamma=90$, $\beta=101.29$, $\alpha=90^\circ$	37.33	222	2.41
	23.23	–602	3.83		43.57	–223	2.08
	35.055	–903	2.56		63.28	822	1.47
	47.287	1105	1.92		75.67	161	1.26
	61.06	628	1.52				
Ni(II)–Cr(III) (g) (LDH) [41] Hexagonal (a : 16.01, b :16.01, c : 7.24 Å), $\gamma=90$, $\beta=90$, $\alpha=120^\circ$	19.206	300	4.63	Ni(II)–Cr(III) (g) (LDH) [46] Monoclinic 2 (a : 5.73, b :5.95, c : 8.31 Å), $\gamma=90$, $\beta=90.4$, $\alpha=90^\circ$	37.09	022	2.42
	36.398	241	2.47		43.52	004	2.08
	47.049	342	1.93		57.52	015	1.6
	61.060	054	1.52		63.29	–224	1.47
Ni(II)–Cr(III) (u) (LDH) [43] Monoclinic 2 (a : 8.43, b :70.9, c : 7.91 Å) $\gamma=90$, $\beta=90.25$, $\alpha=90^\circ$	11.65	140	7.59	Ni(II)–Cr(III) (u) (LDH) [47] Monoclinic 2 (a : 7.74, b :6.27, c : 14.83 Å), $\gamma=90$, $\beta=112.03$, $\alpha=90^\circ$	36.94	–221	2.43
	22.99	0161	3.86		43.46	222	2.08
	34.96	–371	2.56		63.16	142	1.47
	47.106	084	1.93		75.53	–147	1.58
	61.015	034	1.52				

Fig. 3 XRD of original LDH before (B) and after calcination(A): **a** Ni(II)–Cr(III) LDH(B&A); **b** Ni(II)–Cr(III)/a LDH (B and A); **c** Ni(II)–Cr(III)/g (B and A); and **d** Ni(II)–Cr(III)/u LDH (B and A)



electrostatically the most stable [35]. In addition, the (200) (-223) (004) and (222) miller indices at d -spacing 2.08 Å for isolated Ni(II)–Cr(III) LDHs after calcination are calculated using CRYSTALSLEUTH program. The lattice parameters (a , b , c Å) and (γ , β , α°) for the Monoclinic 2, Hexagonal, and Tetragonal phase of Ni(II)–Cr(III) LDHs are listed in Table 2 using a software CRYSTALSLEUTH program [36–39]. The calculated values as well as the detected d values are in a good agreement with the reported data base_code_amcsd [40–47]. In pure Ni(II)–Cr(III) LDHs before calcination, four peaks exist at $2\theta \cong 11$, 22, 35, 47, and 61° , all peaks are weak intense broad peaks. This confirms the semi-crystalline nature of Ni(II)–Cr(III) LDHs. Also, XRD peaks of Ni(II)–Cr(III) LDHs after calcination, the five peaks existing at $2\theta \cong 37$, 43, 63 and 72° , appeared, and the broad peak is shifted to smaller angles that confirms the strong interaction between Ni and Cr LDHs. Finally, the calcination process of Ni(II)–Cr(III) LDHs has a small effect on the original Ni(II)–Cr(III) LDHs crystallinity.

3.4 FESEM analysis of Ni(II)–Cr(III) LDH

The morphologies of the as-prepared samples were explored by field emission scanning electron microscopy (FESEM), as presented in Fig. 4a, b. The specific aim is to investigate the influence of acetamide, glycine, and urea

on the resultant LDH morphology. The study demonstrates that LDHs own several clusters of intercrossed flaky sheets [48]. From the image, it can be noticed that the particle dimension in LDH is located on the non-metric scale.

In comparison of Ni(II)–Cr(III) LDH (Fig. 4a) with Ni(II)–Cr(III) LDH synthesized in the presence of acetamide, glycine, and urea, it is clear to see the difference in surface morphology for the LDH with or without these organic molecules. There is a clear difference in the resulting particles shape of Ni(II)–Cr(III) LDH prepared in the existence of the three organic molecules depending on the nature of these functionalized amino compounds. Figure 4b shows the FESEM of as-prepared Ni(II)–Cr(III) LDH and Ni(II)–Cr(III) LDH prepared in the presence of different organic molecules. From the images, it can be noticed that the porosity between the calcinated clusters is much more than the porosity between the clusters before the calcination process. This may be ascribed to the elimination of water, CO_2 , and intercalated organic molecules between the layered double hydroxide to convert into mixed nickel–chromium oxides during the calcination, which results in establishment of channels and pores [49]. Also from the images, it can be realized that the resulting mixed Ni(II)–Cr(III) oxides from Ni(II)–Cr(III) LDH, Ni(II)–Cr(III)/a, Ni(II)–Cr(III)/g LDH, and Ni(II)–Cr(III)/u are located in the nanoscale.

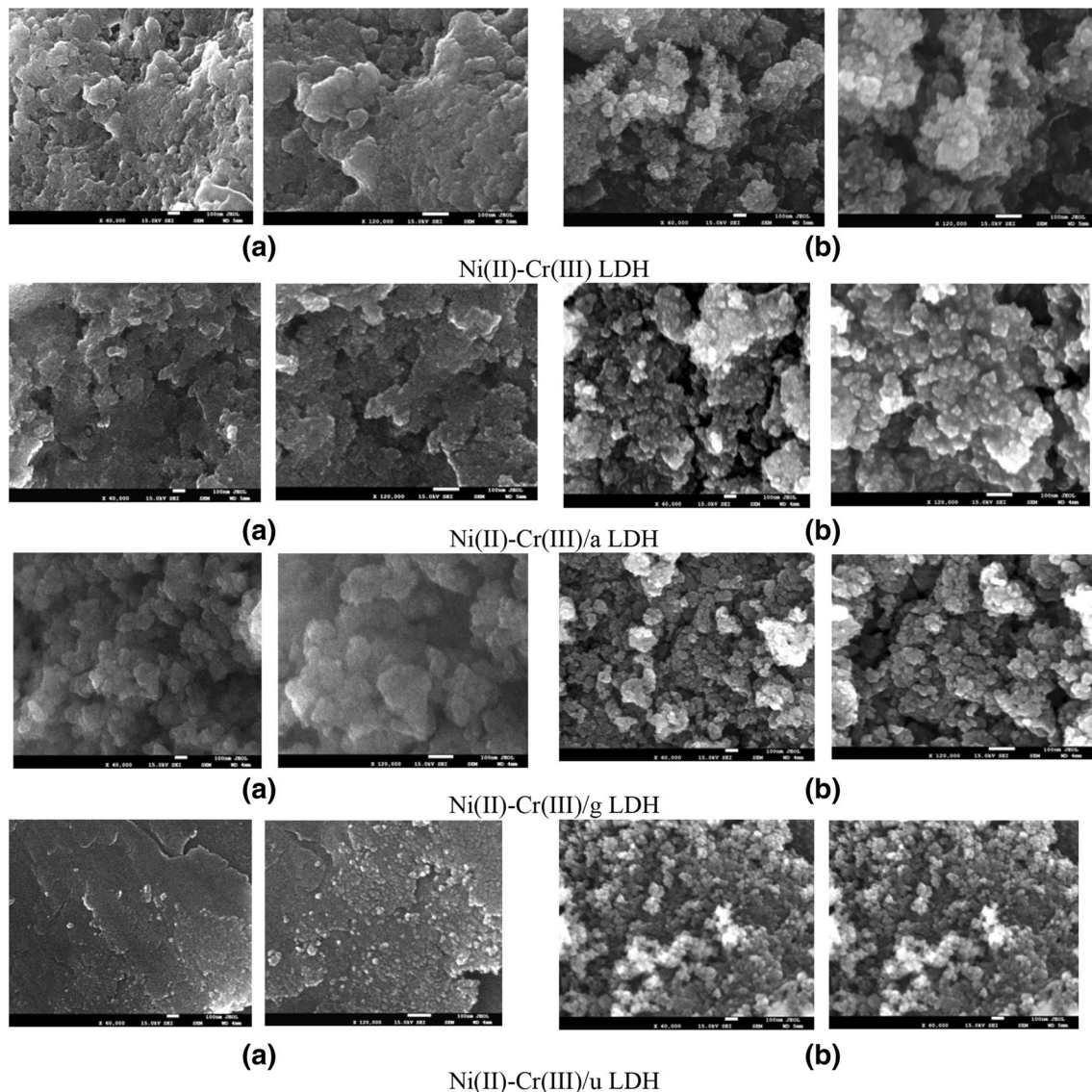


Fig. 4 SEM images of Ni(II)–Cr(III) LDH, Ni(II)–Cr(III)/a LDH, Ni(II)–Cr(III)/g LDH, and Ni(II)–Cr(III)/u LDH at two different magnifications: **a** before and **b** after calcination

3.5 HRTEM analysis of Ni(II)–Cr(III) LDH

TEM was used with the purpose of investigation of the morphology and particle size of mixed Ni(II)–Cr(III) oxides and the product obtained after calcinations at 600 °C for 2.5 h, as presented in Fig. 5. The HRTEM micrographs established that mixed Ni(II)–Cr(III) oxide particles had the representation of the LDH platelet configuration with a reasonably even size of below 10 nm. As displayed in Fig. 5b, aggregates of fine particles were identified after calcination process.

3.6 Photoluminescence properties of Ni(II)–Cr(III) LDHs

The PL spectra exploration is very important to show the relocation, transference, and separation effectiveness of the photo-generated electron and hole pairs in numerous semiconductors [50]. Figure 6 displays the PL spectra of the LDHs samples before calcination. It is observed that a sharp PL emission peak is obtained for all samples at 364 nm, and this can be due to the encirclement of charge transporters typically from excitons on its surface. The maximum

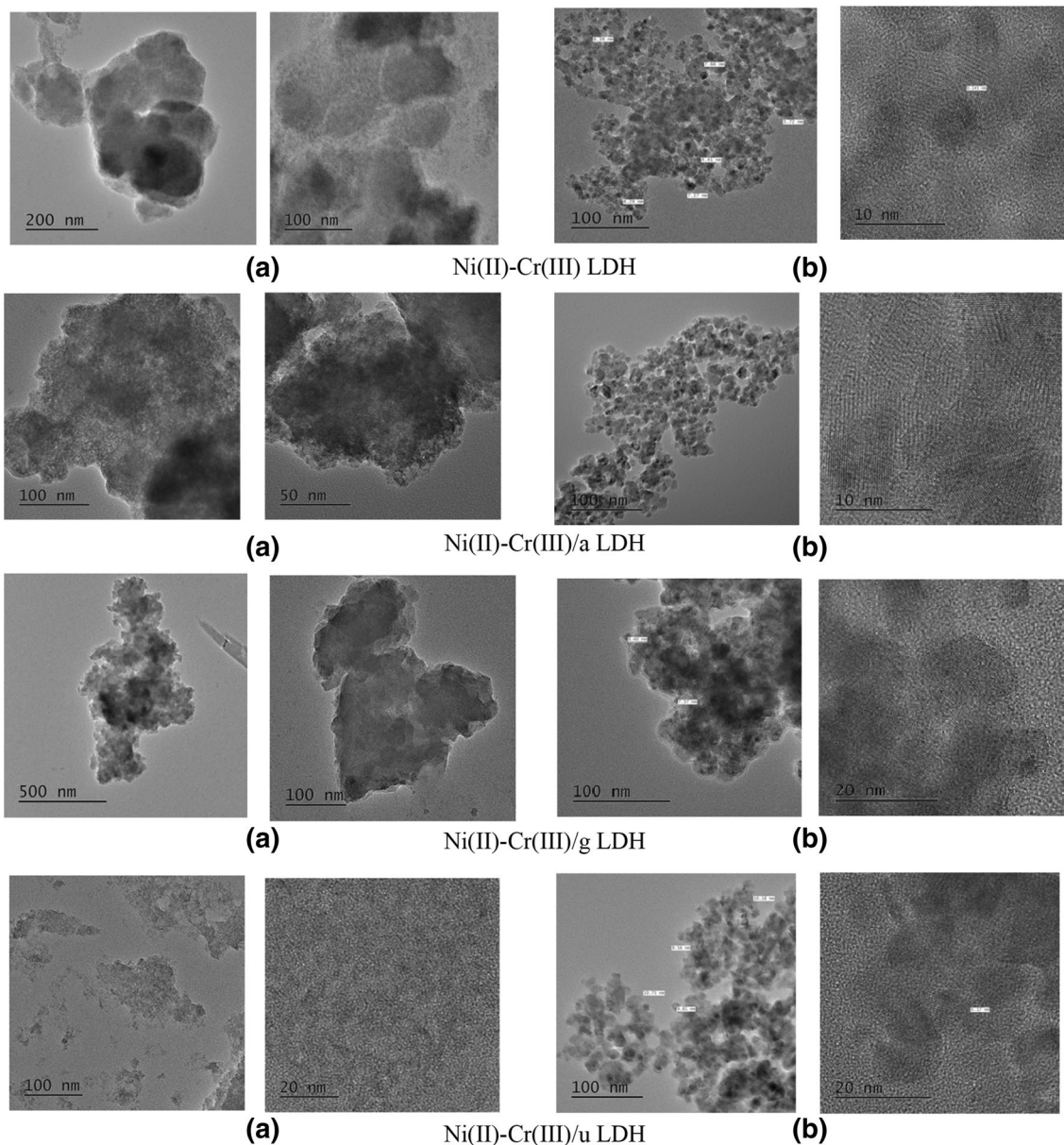


Fig. 5 HRTEM images of Ni(II)–Cr(III) LDH, Ni(II)–Cr(III)/a LDH, Ni(II)–Cr(III)/g LDH, and Ni(II)–Cr(III)/u LDH at two different magnifications: **a** before and **b** after calcination

PL emission peak intensities are recorded as 1361, 939, 819, and 443 for the sample containing acetamide, bare sample, a sample containing urea, and a sample containing glycine, respectively. PL emission broad peak at 468 nm is recorded with peak intensities of 514 for Ni(II)–Cr(III) LDH. By addition of acetamide organic molecule during the preparation of Ni(II)–Cr(III) LDH, an enhancement of broad peak intensity (716) is obtained. On the other hand, in the presence of urea and glycine, the broad peak has been disappeared. Figure 6 shows, that for all samples, symmetrical sharp peaks at $\lambda = 364$ nm without any shifts appeared. There are two main zones for photoluminescence; one is

attributed to band edge emission, which occurs at a shorter wavelength, and the other occurs at a longer wavelength attributable to the capture emission. Davar et. al [51]. and Gadallah et al. [52] have two such reports. Generally, the reduction or intensification of the luminescence intensity is determined by the distance between the nanoparticle Ni and the nanoparticle Cr. When there is no distance or very short distance between nickel and chromium nanoparticles, there is a decrease in luminescence, the so-called luminescence curing. Over a certain distance between the Ni and Cr nanoparticles, there is an increase in luminescence, the so-called luminescence intensification. Both luminescence extinction

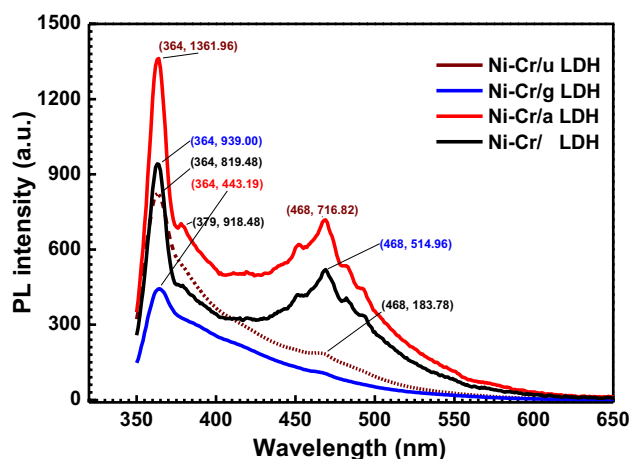


Fig. 6 Photoluminescence emission spectra of Ni(II)-Cr(III)/u LDH, Ni(II)-Cr(III)/g LDH, Ni(II)-Cr(III)/a LDH, and Ni(II)-Cr(III)/LDH (before calcination)

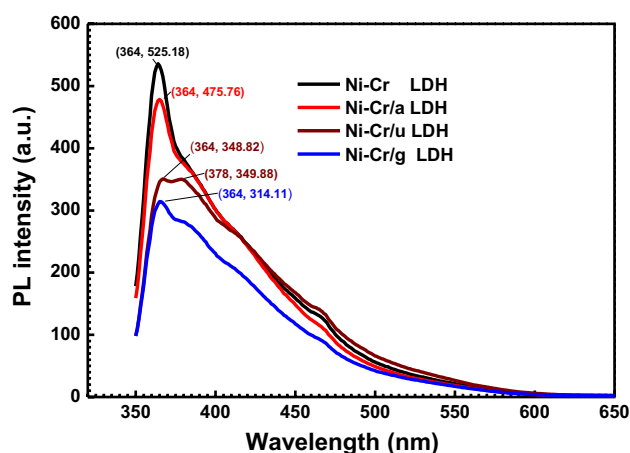


Fig. 7 Photoluminescence emission spectra of Ni(II)-Cr(III) LDH; Ni(II)-Cr(III)/a LDH; Ni(II)-Cr(III)/u LDH; and Ni(II)-Cr(III)/g LDH (after calcination)

and amplification of luminescence have been reported [53]. Thus, the presence of such organic compounds during the preparation stage effects on the PL intensity. This influence is owing to the synergistic behavior of both LDH and different previous organic monomers. Since, the electron transmission is of useful applied importance in some cases such as photocatalysis.

Figure 7 shows the PL spectra of mixed Ni(II)-Cr(III) oxides prepared from LDHs samples after calcination at 600 °C for 2.5 h. We observed the broad PL emission main peak for all investigated LDHs (except Ni(II)-Cr(III)/g LDH) at 364 nm. The Ni(II)-Cr(III)/g LDH polymer shows a shoulder broad peak at both 364 and 378 nm at the same peak intensity. The PL intensity of the resulting mixed Ni(II)-Cr(III) oxides from the LDHs takes the following

order: Ni(II)-Cr(III) LDH (525 PL max.) > Ni(II)-Cr(III)/a LDH (475 PL max.) > Ni(II)-Cr(III)/g LDH (349 PL max.) > Ni(II)-Cr(III)/u LDH (314 PL max.), respectively. Thus, the presence of such organic compounds during the calcination affect the PL intensity. The maximum quenching is observed for mixed Ni(II)-Cr(III) oxides which calcinated from Ni(II)-Cr(III)/u LDH, demonstrating a remarkable reduction of the electron-hole recombination with the maximum photocatalytic activity to visible light-driven H₂ and O₂ evolution, which is consistent with the photocatalytic results.

4 Conclusion

Properties of LDHs before and after calcination are affected by the presence of functionalized amino organic compounds in the starting materials. Presence of the functionalized organic compounds improved the thermal stability of LDHs and changed the crystal types of LDHs before and after calcination which affects the catalytic properties of the resulting mixed metal oxide nanoparticles. A highly porous structure of mixed metal oxides was obtained after calcination process with a semi-crystallinity nature. The presence of functionalized organic compounds during the calcination affects the PL intensity. The PL intensity has been decreased by a factor of 0.1, 0.34, and 0.4 in the presence of acetamide, glycine, and urea, respectively.

References

1. MSh Zoromba, M.A. Nour, H.E. Eltamimy, S.A. Abed El-Mak-soud, Effect of modified layered double hydroxide on the flammability and mechanical properties of polypropylene. *Sci. Eng. Compos. Mater.* **25**, 101–108 (2018)
2. B. Zümreoglu-Karan, A.V. Ahmet Nedim, Layered double hydroxides-multifunctional nanomaterials. *Chem. Pap. Chemicke Zvesti* **66**, 1–10 (2012)
3. S. Wang, C. Bryan, H. Gao, P. I. Phol, C. J. Brinker, K. Yu, H. Xu, Y. Yang, P. S. Braterman, Z. Xu, Potential applications of nanostructured materials in nuclear waste management, *Sandia Natl. Lab. SAND2003-3313*; 2003, 95
4. P. Liu, C. Wang, C. Li, Epoxidation of allylic alcohols on self-assembled polyoxometalates hosted in layered double hydroxides with aqueous H₂O₂ as oxidant. *J. Catal.* **262**, 159–168 (2009)
5. K. Galejová, L. Obalová, K. Jirátořová, K. Pacultová, F. Kovanda, N₂O catalytic decomposition-effect of pelting pressure on activity of Co-Mn-Al mixed oxide catalysts. *Chem. Pap. Chemicke Zvesti* **63**, 172–179 (2009)
6. K. Karásková, L. Obalová, K. Jiratová, F. Kovanda, Effect of promoters in Co-Mn-Al mixed oxide catalyst on N₂O decomposition. *Chem. Eng. J.* **160**, 480–487 (2010)
7. S. Casenave, H. Martinez, C. Guimon, A. Auroux, V. Hulea, E. Dumitriu, Acid and base properties of MgCuAl mixed oxides. *J. Therm. Anal. Calorim.* **72**, 191–198 (2003)
8. M. Park, C. Lee, E.J. Lee, J.H. Choy, J.E. Kim, J. Choi, Layered doublehydroxides as potential solid base for beneficial

- remediation of endosulfan-contaminated soils. *J. Phys. Chem. Solids* **65**, 513–516 (2004)
9. J. Carpentier, J.F. Lemonier, S. Siffert, E.A. Zhilinskaya, A. Aboukais, Characterisation of Mg/Al hydrotalcite with inter-layer palladium complex for catalytic oxidation of toluene. *Appl. Catal. A. Gen.* **234**, 91–101 (2002)
 10. J.H. Choy, J.S. Jung, J.M. Oh, M. Park, J. Jeong, Y.K. Kang, O.J. Han, Layered double hydroxide as an efficient drug reservoir for folate derivatives. *Biomaterials* **25**, 3059–3064 (2004)
 11. F. Leroux, J.P. Besse, Polymer Interleaved Layered Double Hydroxides: A New Emerging Class of Nanocomposites. *Chem. Mater.* **13**, 3507–3515 (2001)
 12. J. Inacio, C. Taviot-Gueho, C. Forano, J.P. Besse, Adsorption of MCPA pesticide by MgAl-layered double hydroxides. *Appl. Clay Sci.* **18**, 255–264 (2001)
 13. Y. You, H. Zhao, G.F. Vance, Adsorption of dicamba (3,6-dichloro-2-methoxy benzoic acid) in aqueous solution by calcined-layered double hydroxides. *Appl. Clay Sci.* **21**, 217–226 (2002)
 14. V. Prévot, B. Casal, E. Ruiz-Hitzky, Intracrystalline alkylation of benzoate ions into layered double hydroxides. *J. Mater. Chem.* **11**, 554–560 (2001)
 15. E. Gardner, K.M. Huntoon, T.J. Pinnavaia, Direct synthesis of alkonide-intercalated derivatives of hydrotalcite-like layered double hydroxides: precursors for the formation of colloidal layered double hydroxide suspensions and transparent thin films. *Adv. Mater.* **13**, 1263–1266 (2001)
 16. M. Ogawa, K. Kuroda, Photofunctions of intercalation compounds. *Chem. Rev.* **95**, 399–438 (1995)
 17. L. Perioli, T. Posati, M. Nocchetti, F. Bellezza, U. Constantino, A. Cipiciani, Intercalation and release of anti-inflammatory drug diclofenac into nanosized ZnAl hydrotalcite-like compound. *Appl. Clay Sci.* **53**, 374–378 (2011)
 18. S.-J. Ryu, H. Jung, J.-M. Oh, J.-K. Lee, J.-H. Choy, Layered double hydroxides as novel antibacterial drug delivery system. *J. Phys. Chem. Solids* **71**, 685–688 (2010)
 19. Z.P. Xu, G.S. Stevenson, C.Q. Lu, G.Q. Lu, P.F. Bartlett, P.P. Gray, Stable suspension of layered double hydroxide nanoparticles in aqueous solution. *J. Am. Chem. Soc.* **128**, 36–37 (2006)
 20. J.A. Gursky, S.D. Blough, C. Luna, C. Gomez, A.N. Luevano, E.A. Gardner, Particle-particle interactions between layered double hydroxide nanoparticles. *J. Am. Chem. Soc.* **128**, 8376–8377 (2006)
 21. P. Gunawan, R. Xu, Synthesis of unusual coral-like layered double hydroxide microspheres in a nonaqueous polar solvent/surfactant system. *J. Mater. Chem.* **18**, 2112–2120 (2008)
 22. Y. Du, G. Hu, D. O'Hare, Nucleation and growth of oriented layered double hydroxides on polymer resin beads. *J. Mater. Chem.* **19**, 1160–1165 (2009)
 23. N.M. Hosny, G. Samir, MSh Zoromba, S. Alghool, doped poly(m-phenylenediamine) (PmPDA): a new precursor for Cr₂O₃ nanoparticles. *Polym. Sci. Ser. B* **59**, 91–96 (2017)
 24. G. Hu, D. O'Hare, Unique layered double hydroxide morphologies using reverse microemulsion synthesis. *J. Am. Chem. Soc.* **127**, 17808–17813 (2005)
 25. M. De Jesús Martínez-Ortiz, E. Lima, V. Lara, J. Mz Vivar, Structural and textural evolution during folding of layers of layered double hydroxides. *Langmuir* **24**, 8904–8911 (2008)
 26. Y. Kuang, L. Zhao, S. Zhang, F. Zhang, M. Dong, S. Xu, Morphologies preparations and applications of layered double hydroxide micro-/nanostructures. *Materials* **3**, 5220–5235 (2010)
 27. MSh Zoromba, M.H. Abdel-Aziz, M. Bassyouni, New microstructured chromium doped poly (*p*-toluidine) as new acid–base sensor and precursor for chromic oxide nanostructured. *Polym. Adv. Tech* **28**, 1743–1749 (2017)
 28. N.M. Hosny, G. Samir, MSh Zoromba, S. Alghool, Poly(*o*-toluidine dihydrochloride): spectral characterization and synthesis of eskolite nanoparticles. *Polym. Plast. Eng.* **56**, 435–442 (2017)
 29. M.Sh. Zoromba, S. Alghool, S. Abdel-Hamid, M. Bassyouni, M. Abdel-Aziz, polymerization of aniline derivatives by K₂Cr₂O₇ and production of Cr₂O₃ nanoparticles. *Polym. Adv. Tech.* **28**, 842–848 (2017)
 30. MSh Zoromba, N. A. E.;-Ghamaz, Dielectrical, electrical conduction properties of doped iron/poly(aniline-co-*o*-anthranilic acid) copolymer and production of magnetite-hematite nanoparticles based on composites as precursor *Materials Express. Mater. Express* **6**, 414–422 (2016)
 31. A.F. Al-Hossainy, H.K. Thabet, M.S. Zoromba, A. Ibrahim, Facile synthesis and fabrication of a poly (ortho-anthranilic acid) emeraldine salt thin film for solar cell applications. *New J. Chem.* **42**, 10386–10395 (2018)
 32. A. Badr, A. El-Amin, A. Al-Hossainy, Elucidation of charge transport and optical parameters in the newly ICR-dppm organic crystalline semiconductors. *J. Phys. Chem. C* **112**, 14188–14195 (2008)
 33. A.F. Al-Hossainy, A. Ibrahim, The effects of annealing temperature on the structural properties and optical constants of a novel DPEA-MR-Zn organic crystalline semiconductor nanostructure thin films. *Opt. Mater.* **73**, 138–153 (2017)
 34. A. Ibrahim, M. Abdel-Aziz, M.S. Zoromba, A. Al-Hossainy, Structural, optical, and electrical properties of multi-walled carbon nanotubes/polyaniline/Fe₃O₄ ternary nanocomposites thin film. *Synth. Meter.* **238**, 1–13 (2018)
 35. O.A. El-Gammal, A.F. Al-Hossainy, S.A. El-Brashy, Spectroscopic, DFT, optical band gap, powder X-ray diffraction and bleomycin-dependant DNA studies of Co (II), Ni (II) and Cu (II) complexes derived from macrocyclic Schiff base. *J. Mol. Struct.* **1165**, 177–195 (2018)
 36. A.F. Al-Hossainy, M.S. Zoromba, R. Hassanien, Eco-friendly method to synthesize and characterize 2D nanostructured (1, 2-bis (diphenyl-phosphino) ethyl) tungsten tetracarbonyl methyl red/copper oxide di-layer thin films. *Bull. Mater. Sci.* **41**, 80 (2018)
 37. A. Al-Hossainy, M.S. Zoromba, New organic semiconductor thin film derived from *p*-toluidine monomer. *J. Mol. Struct.* **1156**, 83–90 (2018)
 38. A.B. Slimane, A.F. Al-Hossainy, M.S. Zoromba, Synthesis and optoelectronic properties of conductive nanostructured poly(aniline-co-*o*-aminophenol) thin film. *J. Mater. Sci: Mater. Electron.* **29**, 8431–8445 (2018)
 39. A.F. Al-Hossainy, A. Ibrahim, Structural, optical dispersion and dielectric properties of novel chromium nickel organic crystalline semiconductors. *Mater. Sci. Semicond. Process* **38**, 13–23 (2015)
 40. H. Horiuchi, A. Saito, T. Tachi, H. Nagasawa, Structure of synthetic Li₂ (Mg, Cu) Cu₂ [Si₂O₆]₂: a unique chain silicate related to pyroxene. *Am. Miner.* **82**, 143–148 (1997)
 41. W. G. Mumme, Weibullite Ag (sub 0.32) Pb (sub 5.09) Bi (sub 8.55) Se (sub 6.08) S (11.92) from Falun, Sweden; a higher homologue of galenobismutite. *Can. Mineral.* **18**(1980) 1–12.
 42. G.E. Hamburger, M.J. Buerger, The structure of tourmaline. *Am. Miner.* **33**, 532–540 (1948)
 43. S.I.L.V.I.O. Menchetti, C.E.S.A.R.E. Sabelli, The crystal structure of baratovite. *Am. Miner.* **64**, 383–389 (1979)
 44. T. Araki, T. Zoltai, Refinement of crystal structure of a glauberite. *Am. Miner.* **52**, 1272 (1967)
 45. W.A. Dollase, Refinement of the crystal structures of epidote, allanite and hancockite. *Am. Miner.* **56**, 447–464 (1971)
 46. G.Y. Chao, Crystal-structure of carletonite-KNA4CA4SI8O18 (CO₃)₄(F, OH) H₂O-double-sheet silicate. *Am. Miner.* **57**, 765 (1972)
 47. S. Nayak, L. Mohapatra, K. Parida, Visible light-driven novel g-C₃N₄/NiFe-LDH composite photocatalyst with enhanced

- photocatalytic activity towards water oxidation and reduction reaction. *J. Mater. Chem. A* **36**, 18622–18635 (2015)
48. N. Balsamo, S. Mendieta, M. Oliva, G. Eimer, M. Crivello, Synthesis and characterization of metal mixed oxides from Layered Double Hydroxides. *Procedia Mater. Sci.* **1**, 506–513 (2012)
 49. X. Guo, F. Zhang, D.G. Evans, X. Duan, Layered double hydroxide films: synthesis, properties and applications. *Chem. Commun.* **46**, 5197–5210 (2010)
 50. L.K. van Vugt, S.J. Veen, E.P.A.M. Bakkers, A.L. Roest, D. Vanmaekelbergh, Increase of the photoluminescence intensity of InP nanowires by photoassisted surface passivation. *J. Am. Chem. Soc.* **127**, 12357–12362 (2005)
 51. F. Davar, M.R. Loghman-Estarki, M. Salavati-Niasari, R. Ashiri, Synthesis of volcano-like CdS/organic nanocomposite. *Int. J. Appl. Ceram. Technol.* **11**, 637–644 (2014)
 52. A.-S. Gadallah, M.M. El-Nahass, Structural, optical constant and photoluminescence of ZnO thin films grown by sol–gel spin coating. *Adv. Cond. Matt. Phys.* **234546**, 11 (2013)
 53. O.G. Tovmachenko, C. Graf, D.J. van den Heuvel, A. van Blaaderen, H.C. Gerritsen, Fluorescence enhancement by metal-core/silica-shell nanoparticles. *Adv. Mater.* **18**, 91–95 (2006)

Publisher's Note Springer Nature remains neutral with regard to jurisdictional claims in published maps and institutional affiliations.

Affiliations

M. Sh. Zoromba^{1,2} · M. Bassyouni^{1,3} · M. H. Abdel-Aziz^{1,4} · Ahmed F. Al-Hossainy^{5,6}  · Numan Salah⁶ · A. A. Al-Ghamdi⁷ · Mohamed R. Eid^{8,9}

¹ Department of Chemical and Materials Engineering, King Abdulaziz University, Rabigh 21911, Saudi Arabia

² Department of Chemistry, Faculty of Science, Port Said University, Port-Said 42521, Egypt

³ Department of Chemical Engineering, Faculty of Engineering, Port Said University, Port Fouad 42521, Egypt

⁴ Department of Chemical Engineering, Faculty of Engineering, Alexandria University, Alexandria, Egypt

⁵ Department of Chemistry, Faculty of Science, New Valley University, El-kharga, Al-Wadi Al-Jadid 72511, Egypt

⁶ Department of Chemistry, Faculty of Science, Northern Border University, Arar 1321, Saudi Arabia

⁷ Centre of Nanotechnology, King Abdulaziz University, Jidda 21589, Saudi Arabia

⁸ Department of Mathematics, Faculty of Science, New Valley University, El-kharga, Al-Wadi Al-Jadid 72511, Egypt

⁹ Department of Basic Science, Deanship of Preparatory Year, Northern Border University, Arar 91431, Saudi Arabia